An Equatorial–Extratropical Dipole Structure of the Atlantic Niño

HYACINTH C. NNAMCHI,[a] JIANPING LI,[b] FRED KUCHARSKI,[c] IN-SIK KANG,[d,e] NOEL S. KEENLYSIDE,[f,g] PING CHANG,[h,i] AND RICCARDO FARNETI[c]

[a] *Department of Geography, University of Nigeria, Nsukka, Nigeria*
[b] *College of Global Change and Earth System Science, Beijing Normal University, and Joint Center for Global Change Studies, Beijing, China*
[c] *Earth System Physics Section, Abdus Salam International Centre for Theoretical Physics, Trieste, Italy*
[d] *School of Earth and Environmental Sciences, Seoul National University, Seoul, South Korea*
[e] *Center of Excellence for Climate Change Research, King Abdulaziz University, Jeddah, Saudi Arabia*
[f] *Geophysical Institute, University of Bergen, Bergen, Norway*
[g] *Bjerknes Centre for Climate Research, Bergen, Norway*
[h] *Department of Oceanography, Texas A&M University, College Station, Texas*
[i] *Collaborative Innovation Center of Marine Science and Technology, Ocean University of China, Qingdao, China*

(Manuscript received 16 December 2015, in final form 8 March 2016)

ABSTRACT

Equatorial Atlantic variability is dominated by the Atlantic Niño peaking during the boreal summer. Studies have shown robust links of the Atlantic Niño to fluctuations of the St. Helena subtropical anticyclone and Benguela Niño events. Furthermore, the occurrence of opposite sea surface temperature (SST) anomalies in the eastern equatorial and southwestern extratropical South Atlantic Ocean (SAO), also peaking in boreal summer, has recently been identified and termed the SAO dipole (SAOD). However, the extent to which and how the Atlantic Niño and SAOD are related remain unclear. Here, an analysis of historical observations reveals the Atlantic Niño as a possible intrinsic equatorial arm of the SAOD. Specifically, the observed sporadic equatorial warming characteristic of the Atlantic Niño (~0.4 K) is consistently linked to southwestern cooling (~−0.4 K) of the Atlantic Ocean during the boreal summer. Heat budget calculations show that the SAOD is largely driven by the surface net heat flux anomalies while ocean dynamics may be of secondary importance. Perturbations of the St. Helena anticyclone appear to be the dominant mechanism triggering the surface heat flux anomalies. A weakening of the anticyclone will tend to weaken the prevailing northeasterlies and enhance evaporative cooling over the southwestern Atlantic Ocean. In the equatorial region, the southeast trade winds weaken, thereby suppressing evaporation and leading to net surface warming. Thus, it is hypothesized that the wind–evaporation–SST feedback may be responsible for the growth of the SAOD events linking southern extratropics and equatorial Atlantic variability via surface net heat flux anomalies.

1. Introduction

Tropical Atlantic variability exerts profound impacts on atmospheric circulation, latitudinal migration of the intertropical convergence zone, hydrological cycle, hurricane development, and marine ecosystems (Giannini et al. 2003; Xie and Carton 2004; Subramaniam et al. 2013; Patricola et al. 2014; Siongco et al. 2015). Thus, the tropical Atlantic Ocean is often implicated in climate variability over parts of the adjacent continents including the Guinea coast, the Sahel, and Brazil Nordeste. Studies suggest that during the boreal summer [June–August (JJA)], tropical Atlantic variability is dominated by the equatorial zonal mode termed the Atlantic Niño occurring at the interannual time scale (Zebiak 1993; Chang et al. 2006; Keenlyside and Latif 2007; Brandt et al. 2011). The peak phase of the Atlantic Niño in JJA is characterized by a relaxation of the southeast trade winds and zonally oriented anomalous warming along the climatological mean axis of the cold tongue.

There are also two off-equatorial modes in the Atlantic Ocean. One, peaking in boreal spring, is the interhemispheric meridional sea surface temperature (SST) gradient linked to cross-equatorial winds referred to as the Atlantic meridional mode (Carton et al. 1996; Chang et al. 1997;

Corresponding author address: Dr. Hyacinth C. Nnamchi, Department of Geography, University of Nigeria, Russ Bldg., Nsukka 410001, Nigeria.
E-mail: hyacinth.nnamchi@unn.edu.ng

DOI: 10.1175/JCLI-D-15-0894.1

Patricola et al. 2014). Fluctuations in the meridional mode preceded Atlantic Niño during certain periods (Servain et al. 1999), although the two are generally regarded as independent modes of variability. The other off-equatorial mode—referred to as the South Atlantic subtropical dipole (SASD)—manifests itself as subtropical SST anomalies off the African coast associated with opposite phase farther south off the coast of South America and is linked to fluctuations of the St. Helena subtropical anticyclone (Venegas et al. 1996, 1997; Haarsma et al. 2005; Colberg and Reason 2007; Morioka et al. 2011). The SASD peaks in boreal winter [December–February (DJF)] (Venegas et al. 1997; Morioka et al. 2011) and the northern arm is typically located away from the equator at about 15°–25°S (Morioka et al. 2011, 2014). Thus, neither Atlantic meridional mode nor the SASD coincides with the Atlantic Niño in either space or season.

However, the seasonally stratified observational analysis of Nnamchi et al. (2011) suggests that, in some years, equatorial warming anomalies characteristic of the Atlantic Niño may be associated with cooling of similar magnitudes in the southwestern Atlantic off the Brazil–Uruguay–Argentina coast during JJA. This SST anomaly pattern marks the positive phase of the phenomenon termed the South Atlantic Ocean dipole (SAOD). The negative phase of the SAOD is characterized by a reversal of the pattern, with cooling anomalies in the Atlantic Niño region [the northeast pole (NEP)] and warming over the southwest pole (SWP) off the coast of South America. Consistent with this, Trzaska et al. (2007) analyzed SST anomalies simulated by a thermodynamic ocean model and showed (using slightly different but overlapping spatial domains) that a dipole structure peaking in July–September is the dominant mode of SST variability in the South Atlantic Ocean. Indeed, boreal summer precipitation at the Guinea coast of Africa that is traditionally associated with the Atlantic Niño (Wagner and Da Silva 1994; Giannini et al. 2003; Tokinaga and Xie 2011) is actually correlated with SAOD-type SST variability (Nnamchi and Li 2011, 2016; Nnamchi et al. 2013).

Previous studies implicate a wave-driven SST response with perturbations of the St. Helena anticyclone acting as an external factor in Atlantic Niño evolution. Lübbecke et al. (2014) discussed this in terms of wind energy, which is one method of looking at dynamically driven responses. Perturbations of the anticyclone are driven by monsoonal heating over the adjacent continents and are amplified by local air–sea interactions (Seager et al. 2003; Richter et al. 2008). A weakening of the St. Helena anticyclone could induce large-scale circulation anomalies associated the Benguela Niño in boreal spring and the Atlantic Niño in JJA (Lübbecke et al. 2010; Richter et al. 2010; Lübbecke et al. 2014). The mechanism causing the Benguela Niño has been attributed to dynamically driven propagation of Kelvin waves from the equatorial region (Florenchie et al. 2003, 2004; Lübbecke et al. 2010, 2014), the localized effects of winds anomalies (Richter et al. 2010), and variations in cloud feedbacks (Huang and Hu 2007; Bellomo et al. 2015). On the other hand, the Atlantic Niño is widely believed to be dynamically driven because of the Bjerknes feedback (Zebiak 1993; Keenlyside and Latif 2007; Lübbecke and McPhaden 2013; Deppenmeier et al. 2016), equatorial Kelvin waves (Brandt et al. 2011), and meridional temperature advection from the tropical North Atlantic Ocean (Richter et al. 2013).

The present study is motivated by a recent modeling analysis focusing on the Atlantic Niño region (Nnamchi et al. 2015, hereafter N15), which concluded that thermodynamic processes can explain the SST anomalies to a first order, contrary to the previous studies. The possible role of the St. Helena anticyclone was suggested but not shown. Earlier studies linking perturbations of the anticyclone to the evolution of eastern equatorial Atlantic SST anomalies show that the Benguela Niño and Atlantic Niño are so strongly correlated that they may be considered the same mode (Lübbecke et al. 2010; Richter et al. 2010). The NEP region (0°–15°S, 10°E–20°W) of the SAOD actually encompasses both Niños.

Against the above background, here we address the following question: What is the relationship between the Atlantic Niño peaking in JJA and ocean–atmosphere anomalies over the South Atlantic extratropics? Lübbecke et al. (2010, 2014) demonstrated that there is a robust connection between the Atlantic Niño and fluctuations of the St. Helena anticyclone, which can act as an external factor in exciting equatorial variability that is further amplified by dynamical ocean–atmosphere interactions. Furthermore, an earlier analysis suggested that the equatorial Atlantic Niño may be a different mode from the SAOD (Nnamchi et al. 2011). We note here that the Atlantic Ocean is subject to large-scale warming trends, giving rise to a weakening of the cold tongue and Niño-like warming pattern in historical observations and numerical simulations (Deser et al. 2010; Tokinaga and Xie 2011), and this may obscure the intrinsic variability. Thus, how the data are preprocessed will affect the characterization of the equatorial and southern Atlantic SST anomaly types.

Here we show that the warming trend in historical observations is not linear. We then account for the observed warming trends and investigate the connection between ocean–atmosphere interactions over equatorial and southern Atlantic Ocean, using ocean reanalysis datasets. We demonstrate that the equatorial Atlantic Niño may actually represent an equatorial arm of the

SAOD, largely driven by surface net heat flux anomalies. Thus, although using different spatial domains, the present study provides observational evidence to support the analysis of N15, which was based on numerical model experiments. Furthermore, we describe the large-scale context that could condition the thermodynamic air–sea interactions driving SST anomalies over the equatorial Atlantic Ocean.

The rest of this paper is organized in four sections. Section 2 describes the observational and reanalysis datasets analyzed. Section 3 examines and compares the indices of the Atlantic Niño and SAOD in space, time, and frequency domains. Section 4 describes the physical mechanism—largely thermodynamic feedbacks that could drive the SAOD-type SST anomalies. Finally, the paper ends with concluding remarks in section 5.

2. Data and methods

a. Observational and reanalysis datasets

Three different observational SST datasets were analyzed. These are the National Oceanic Atmospheric Administration Extended Reconstructed SST (ERSST), version 3b, available at 2° × 2° longitude–latitude grids (Smith et al. 2008); the Hadley Centre Sea Ice and Sea Surface Temperature, version 1, at 1° × 1° (Rayner et al. 2003); and the Kaplan extended SST, version 2, at 5° × 5° (Kaplan et al. 1998).

Sea level pressure and 10-m zonal and meridional wind datasets at 2° × 2° longitude–latitude grids were taken from the Twentieth Century Reanalysis, 1871–2012 (Compo et al. 2011). The depth of the 20°C isotherm, sea surface height, mixed layer depth, zonal currents, meridional currents, and 0–300-m mean and three-dimensional ocean temperature datasets were taken from the European Centre for Medium-Range Weather Forecasts operational Ocean Reanalysis System 3 (ORAS3) for the period 1959–2009 (Balmaseda et al. 2008). The ORAS3 is based on the Hamburg Ocean Primitive Equation model at 1.0° × 1.0° grids with 0.3° equatorial refinement and 29 vertical levels.

The fine equatorial grids of ORAS3 are important in resolving the dynamical ocean–atmosphere feedbacks in the equatorial Atlantic Ocean. Nevertheless, to test the stability of the results, we repeated the heat budget analysis using version 2 of the German contribution to Estimating the Circulation and Climate of the Ocean (GECCO2) reanalysis available at 1.0° × 1.0° horizontal grids and 50 vertical levels (Köhl 2015).

b. SST data filter

The leading empirical orthogonal function (EOF) mode carries approximately 25% of the ensemble mean observed variance of the global SST anomalies, and while there are some differences among datasets, they all show warming trends in JJA. The spatial patterns suggest that the trends are very pronounced over the Atlantic Ocean in the individual datasets and their ensemble mean (Figs. 1a–d). These plots are essentially consistent with the trend maps of Deser et al. (2010) determined based on annual datasets and suggest that the South Atlantic extratropics may have warmed as much as the equatorial Atlantic Ocean over the past decades. For each dataset and the ensemble mean, the time evolution of the leading EOF is plotted on the same axis with the time series of the weighted basin-averaged SST anomaly (WBA) over the South Atlantic Ocean (Figs. 1e–h; the weights applied were determined as the cosine of the gridpoint latitudes). The two time series are strongly correlated ($r = \sim 0.90$), corresponding to R^2 of 0.81. This implies that the global SST anomalies dominated by warming trends explain approximately 81% of the observed JJA variability of WBA.

As shown in Figs. 1e–h, the WBA is obviously composed of some intrinsic interannual and decadal components (see also Martín-Rey et al. 2014), in addition to the long-term secular warming trend. However, the variability of the WBA is not linear and therefore merely subtracting the linear trends from the datasets may not be an effective way to extract the intrinsic variability. Thus, in order to isolate the intrinsic interannual variability from the low-frequency component of the WBA, we filtered the SST anomaly fields as follows:

$$\mathrm{SST}'_{\mathrm{filtered}} = \mathrm{SST}'_{\mathrm{raw}} - \mathrm{WBA}_{\mathrm{low.freq}}, \tag{1}$$

where $\mathrm{SST}'_{\mathrm{raw}}$ and $\mathrm{SST}'_{\mathrm{filtered}}$ denote the raw and filtered SST anomaly datasets, respectively, and $\mathrm{WBA}_{\mathrm{low.freq}}$ is the low-frequency component (determined as the 29-yr running mean at every grid point) of the raw SST anomaly datasets. Subsequent analyses are then based on the filtered datasets, except where otherwise stated. The 29-yr cutoff limit was chosen since the spectral coherence of the Atlantic Niño and southern extratropics is statistically significant up to around 29 years (see section 3b).

c. Atlantic Niño and SAOD indices

Following Zebiak (1993), the Atlantic Niño (ATL3) index was calculated as the domain-averaged SST anomalies over the equatorial Atlantic sector (3°N–3°S, 0°–20°W). The NEP index is averaged over 0°–15°S, 10°E–20°W and the SWP over 25°–40°S, 10°–40°W (Nnamchi et al. 2011). The SAOD index is determined as

$$\mathrm{SAODI} = [\mathrm{SSTA}]_{\mathrm{NEP}} - [\mathrm{SSTA}]_{\mathrm{SWP}}, \tag{2}$$

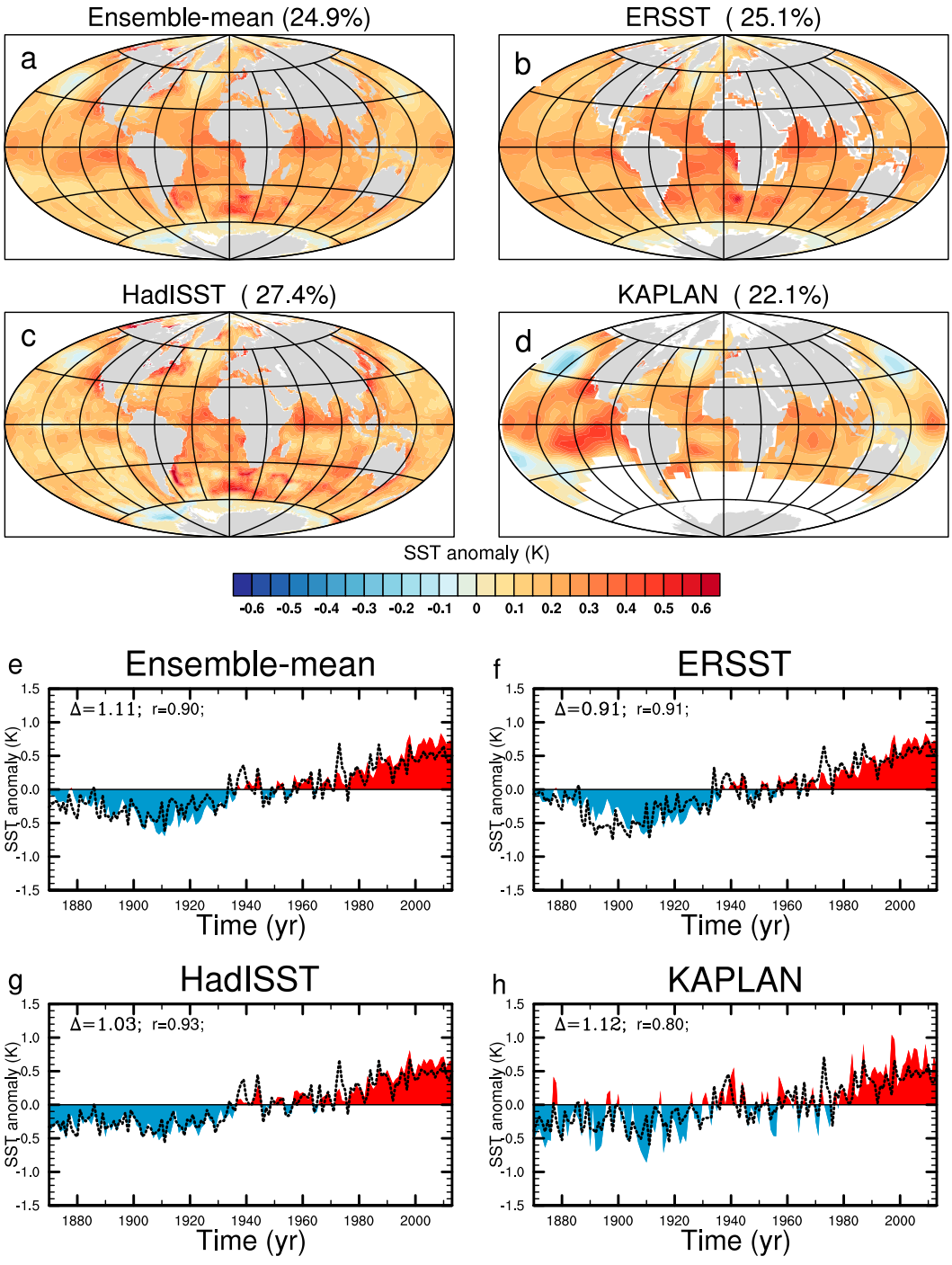

FIG. 1. (a)–(d) Leading EOF of observed global SST variability for JJA 1870–2013 and (e)–(h) the associated time series. The ensemble mean is created from a bilinear interpolation of the three datasets onto 1° × 1° latitude–longitude grids. The variance associated with the leading mode is indicated for each dataset and their ensemble mean in (a)–(d). For (e)–(h), the blue or red color fill shows the time evolution of the EOF time series; the dashed black line shows the WBA. The regression Δ of the EOF time series (as the independent variable) against WBA (as the dependent variable) and their correlation coefficients r are shown in (e)–(h).

where square brackets represent SST anomalies averaged over the domains indicated by the subscripts.

3. Connections between the equatorial and extratropical South Atlantic variability

a. *Ocean–atmosphere anomalies associated with the indices of the Atlantic Niño and SAOD*

The occurrence of the Atlantic Niño can be inferred from ocean–atmosphere changes detectable in the surface winds, ocean heat content (OHC), sea surface height (SSH), and thermocline (e.g., Keenlyside and Latif 2007). Thus, we first compare the variability of these parameters associated with the Atlantic Niño and SAOD indices during JJA when both typically peak.

The regression of the filtered SST anomalies on the ATL3 index from 1870 to 2013 during JJA reveals a robust ($P < 0.001$) anomalous cooling response over the SWP, in addition to the well-known anomalous warming over the NEP (Fig. 2a), creating a dipole. This pattern is reproduced by the SAOD index, with closely aligned meridional axes of maximum and minimum SST anomalies. Physically consistent with the SAOD-type SST variability are large-scale ocean–atmosphere changes characterized by near-surface low-pressure anomalies. The thermocline, defined as the depth of the 20°C isotherm, deepens by about 4 m in the eastern equatorial Atlantic associated with an increase of approximately 436 MJ m^{-3} in OHC per unit volume integrated over the top 300 m (Fig. 2b). At the SWP where the OHC is markedly decreased (~ -376 MJ m^{-3}), the thermocline shoals by about -11 m. As a broad indicator of oceanic circulation, the SSH exhibits a robust response at the NEP but not at the SWP.

As shown by the significance limits in Fig. 2, the SAOD-type SST, surface winds, OHC, SSH, and thermocline anomalies are closely matched by those of the Atlantic Niño. The maximum SST anomaly hinges on the African coast at around 10°S, consistent with the increasing realization that the Atlantic Niño is not purely equatorial but is instead tied to the Benguela Niño phenomenon (Hu and Huang 2007; Lübbecke et al. 2010; Richter et al. 2010).

How reliable are the results shown in Fig. 2 given that the South Atlantic Ocean is often considered sparsely sampled during much of the nineteenth and twentieth centuries? As summarized in Table 1, earlier observational studies based on more recent periods with generally improved observational coverage consistently show the occurrence of a dipole mode in the South Atlantic Ocean. The dipole tends to appear as the second EOF mode in raw datasets, whereas the first mode represents basin-scale uniform anomalies, possibly dominated by warming trends. Thus, in those studies that the linear trends were removed from the SST anomalies prior to the EOF analysis, the dipole clearly emerges as the first mode. A leading dipole mode has also been shown in numerical modeling studies of the South Atlantic SST anomalies (e.g., Colberg and Reason 2007; Morioka et al. 2011).

As the ocean and atmosphere in the region are strongly dependent, the intrinsic variability may be better understood in a coupled framework. Not surprisingly, those studies that analyzed the covariability of oceanic and atmospheric fields report a dipole structure as the leading mode over the South Atlantic Ocean in observations and numerical modeling analyses (Venegas et al. 1996, 1997; Haarsma et al. 2005; Trzaska et al. 2007; Nnamchi et al. 2011). While most of these previous studies are based on monthly anomalies, the seasonally stratified analysis of Nnamchi et al. (2011) reveals that, rather than a solitary equatorial Atlantic Niño, a dipole mode—the SAOD—actually dominates the equatorial and South Atlantic Ocean region during JJA.

Thus, although the SST at the SWP exhibits strongest variability in DJF, it also has a secondary peak (which appears slightly more defined in the filtered datasets) in JJA that coincides with the primary peak of the Atlantic Niño or the NEP [Fig. 3; see also Fig. 2 of Nnamchi et al. (2011)]. In fact, JJA is the only season during which the magnitudes of the SST variability at both poles are comparable, as expected for a dipole mode.

b. *Coherence of eastern equatorial and southwestern extratropical Atlantic SST anomalies*

Spectral and composite analyses are performed to further investigate the relation between the two poles of the SAOD. The spectrum of the Atlantic Niño is consistent with a first-order autoregressive process [AR(1); Fig. 4a], similar to N15. The SWP index has spectral characteristics similar to the Atlantic Niño, but with a more pronounced decadal peak slightly exceeding the AR(1) at 95% confidence level; this appears to enhance the energy in the SAOD spectrum. Interestingly, the cross spectrum shows that the Atlantic Niño and SWP are coherent at $P \leq 0.001$ on the interannual (2.0–3.3 yr) and decadal (12.0–28.8 yr) time scales (Fig. 4b). The phase lag is generally close to $\pm 180°$ where the coherence is robust, suggesting that the variability of the eastern equatorial and southwestern subtropical Atlantic Ocean tend to coincide with each other, but with opposite sign. The analysis here focuses on the interannual variability of these regions that peaks in JJA. The decadal variability will be described in a subsequent study.

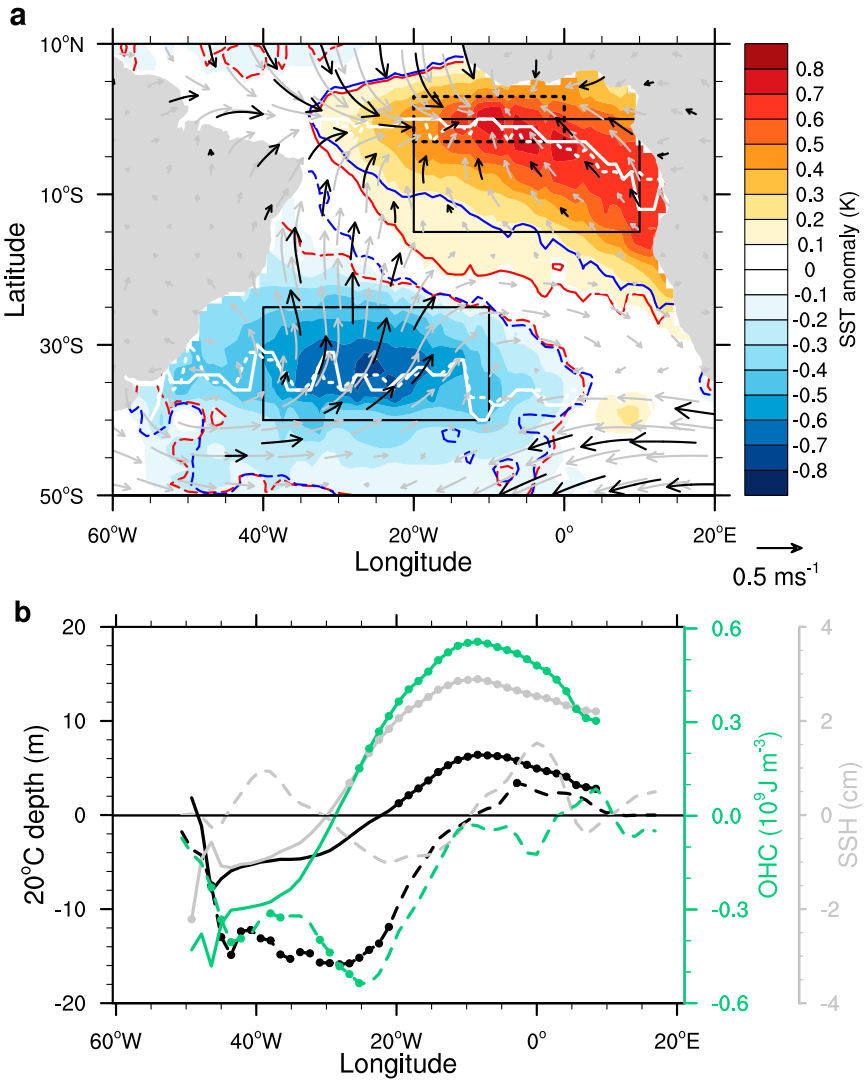

FIG. 2. (a) Observed SST (color scale) and reanalysis surface wind (arrows) anomalies regressed on the SAOD index (1871–2012). Blue (red) curves delineate regressed SST anomalies statistically significant ($P \leq 0.001$) on the ATL3 (SAOD) index; solid (dashed) white curves show the axes of meridional maximum and minimum SST anomalies with respect to the ATL3 (SAOD) index. The black arrows denote regressed wind anomalies significant ($P \leq 0.05$) on both the ATL3 and SAOD indices. Boxes show the ATL3, NEP, and SWP domains. (b) Equatorial (2°N–2°S, solid curves) and extratropical (28°–32°S, dashed curves) thermocline depth (black), OHC (green), and SSH (gray) anomalies regressed on the SAOD index (1960–2009). Dots indicate statistically significant ($P \leq 0.05$) regressions on both the ATL3 and SAOD indices. All plots are based on JJA mean anomalies.

A composite analysis shows that the SAOD occurred 43 out of the 144 years (1870–2013) during JJA in all three datasets analyzed, with comparable tropical (+0.40 K) and subtropical (−0.39 K) mean SST deviations, but no solitary equatorial or subtropical event was found. When we restrict the analysis to the 50-yr period from 1960 to 2009 discussed in section 4, then the SAOD occurred 18 in years; the mean SST deviations remain largely unchanged (at ~0.40 K), but there are two solitary equatorial and one subtropical events (Table 2). This suggests that the results may be affected by the length of data analyzed or the observational period used to construct the SST anomalies, which may slightly weaken the anomalies at one of the poles. Nevertheless, the SAOD clearly dominates irrespective of the period analyzed or the cutoff limit used to filter the datasets. From 1960 to 2009, the negative phase occurred more frequently (in 11 years compared to the

TABLE 1. Dipole modes determined by EOF analysis of the SST anomalies over South Atlantic Ocean in different observations, reported in the previous studies indicated. Shown are the datasets, periods, and spatial domains analyzed by the various studies and how the SST anomalies were preprocessed prior to the EOF analysis, as well as the EOF mode corresponding to the dipole SST anomalies and the associated variance.

Reference	Data	Period	Domain	Anomalies	Mode	Variance (%)
Venegas et al. (1997)	ICOADS	1953–92	0°–50°S, 70°W–20°E	Raw	2	16.7
Sterl and Hazeleger (2003)	NCEP–NCAR	1949–2000	0°–45°S, 75°W–45°E	Detrended	1, 2	28.5, 16.7
Morioka et al. (2011)	HadISST	1960–2008	10°–50°S, 60°W–20°E	Detrended	1	20.4
Nnamchi et al. (2011)	HadISST	1950–2006	5°N–45°S, 60°W–20°E	Raw	1, 2	30.7, 13.2
Nnamchi et al. (2011)	ERSST	1950–2008	5°N–45°S, 60°W–20°E	Raw	2	13.7

positive phase, which occurred only in 7 years) with a greater tendency to persist for some years, for example, 1976–78 and 1982/83. Overall, the frequency of the SAOD determined by the composite analysis represents an occurrence every 3.3 yr during 1870–2013 and 2.8 yr during 1960–2009. As shown in Fig. 4a, the SST spectra have power consistent with an AR(1) process in the 2–5-yr band.

4. Physical mechanisms

a. *Relative contributions of temperature advection and heat flux to the SAOD evolution*

While a robust connection has been established between the eastern equatorial and southwestern extratropical Atlantic SST anomalies, the mechanisms linking the ocean–atmosphere anomalies at the two poles and their evolution are not yet clear. In this section, we explore the governing physical mechanisms through the analysis of the heat budget evolution that drives the SST anomalies at both centers of action, using the more recent period (1960–2009) with generally improved observational coverage. We use the SAOD index derived from the HadISST observations and the ocean reanalysis datasets, which are essentially constrained by observations. The aim is to assess to which extent the results are consistent with the modeling analysis of N15 based on the Atlantic Niño index, having shown above the similarities in other aspects of the observed Atlantic Niño and the SAOD.

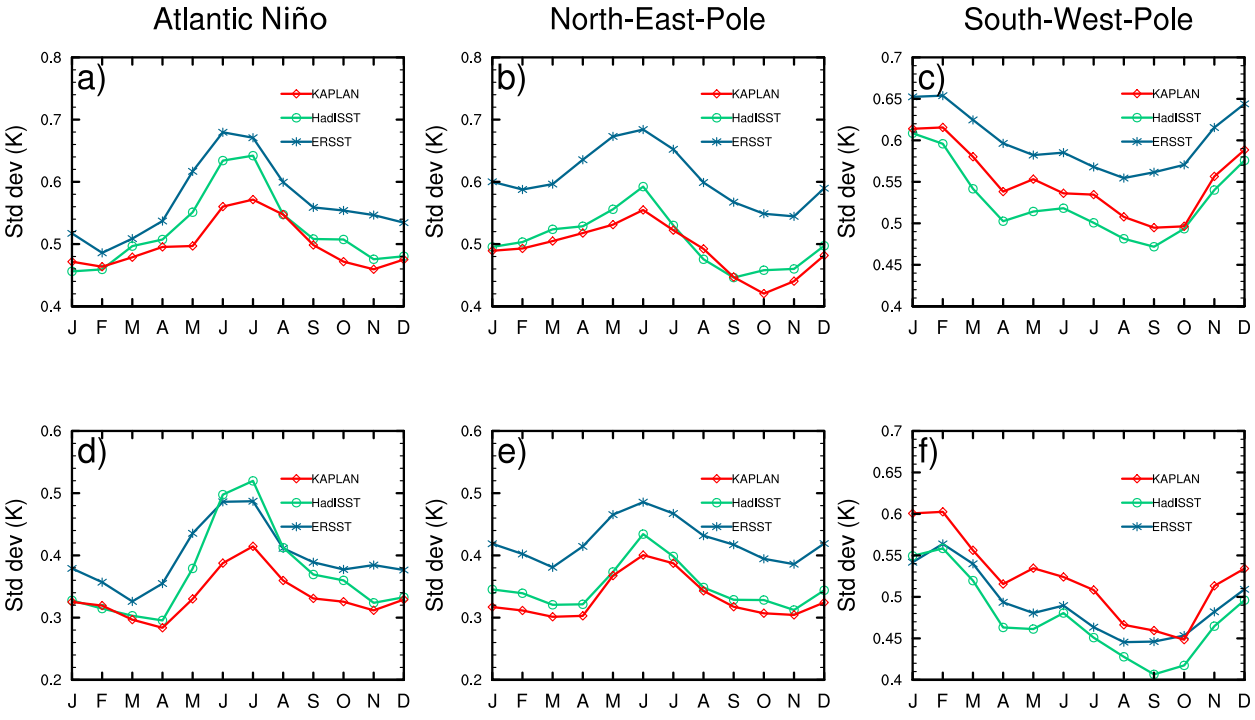

FIG. 3. Observed standard deviation of domain-averaged SST anomalies (1870–2013) over the (a),(d) ATL3, (b),(e) NEP, and (c),(f) SWP. Curves are based on the ERSST (blue), HadISST (green), and Kaplan (red) datasets. The numbers are computed using raw datasets in (a)–(c) and are based on filtered datasets in (d)–(f). Note that the magnitudes of the ATL3 and NEP variability are similar to that of the SWP only during JJA as expected for a dipole mode.

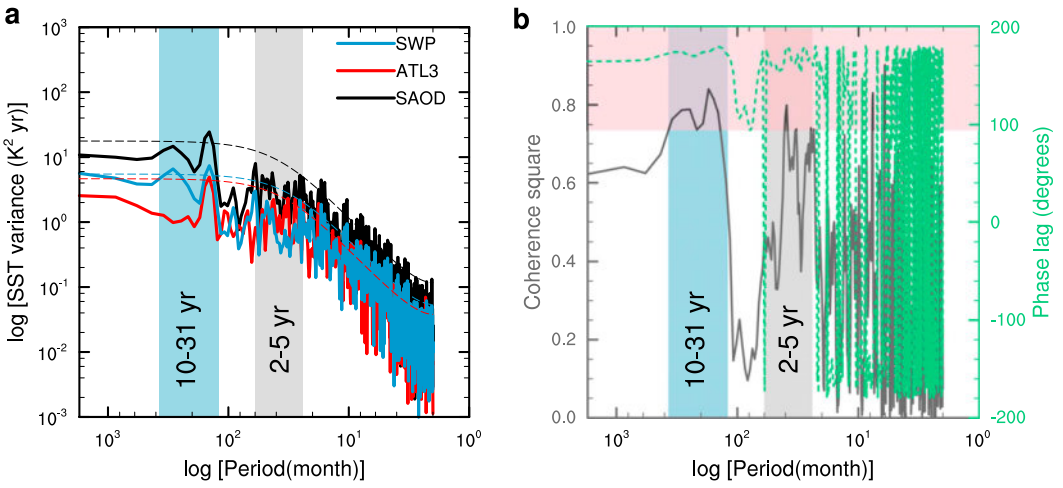

FIG. 4. Comparison of the monthly spectra of the eastern equatorial and southwestern Atlantic SST anomalies, 1870–2013. (a) Solid curves are spectra of the SAOD (black), SWP (blue), and ATL3 (red) indices. Thin dashed curves show 95% confidence level above the theoretical AR(1) spectra. (b) The black curve is the spectral coherence between the ATL3 and SWP indices; transparent pink shading shows statistical significance ($P \leq 0.001$). The dashed green curve shows the phase lag between the ATL3 and SWP indices. The SWP leads at positive lags, ATL3 leads at negative lags, and the two time series evolve together at a phase lag of ~180°. To minimize leakages from strong spectral peaks, 10% of each index time series was tapered prior to computing the spectrum. For display, the spectral estimates were smoothed by three-point Daniell filter while the cospectrum was smoothed by a seven-point filter. In both panels, the vertical bars show the interannual (2–5 yr) and decadal (10–31 yr) variations.

Generally, SST anomalies are driven by a combination of surface net heat flux and three-dimensional temperature advection within the ocean mixed layer. During the course of the year, the ocean mixed layer depth (MLD) at the NEP typically fluctuates from a minimum of around 40 m in March to a maximum of around 55 m by September. On the other hand, the MLD at the SWP exhibits stronger seasonality ranging from about 37 m in February to about 156 m in September (Figs. 5a,b). These represent huge seasonal differences in the evolution of the MLD at the two centers of action. As a result, we explicitly account for the MLD variations at each pole in computing the relative contributions of the surface net heat flux and ocean temperature advection in causing the SAOD-type SST anomalies.

The time rate of the temperature change (tendency, $\partial T/\partial t$) averaged in the ocean mixed layer may be written as follows:

$$\frac{\partial [T]}{\partial t} = \frac{Q_{\text{net}}}{\rho C_w h} - \left[u\frac{\partial T}{\partial x}\right] - \left[v\frac{\partial T}{\partial y}\right] + \text{Res}, \qquad (3)$$

where ρ and C_w are constants representing the seawater density and specific heat capacity of ocean water ($\rho = 10^3\,\text{kg}\,\text{m}^{-3}$ and $C_w = 4 \times 10^3\,\text{J}\,\text{kg}^{-1}\,\text{K}^{-1}$), respectively; T is the SST; and Q_{net} denotes the net heat flux at the ocean surface. The first term on the right-hand side of the equation is subsequently referred to as the heat flux term. The u and v are the horizontal ocean current velocities, and the second and third terms on the right-hand side of Eq. (3) represent the zonal and meridional

TABLE 2. Equatorial–extratropical South Atlantic Ocean SST anomaly types, 1870–2013 and 1960–2009. Classification is based on $\pm 1.0\sigma$ and must occur in all three datasets, and in addition, for dipole 0.5σ must come from the tropics (NEP) and extratropics (SWP) each. The number of occurrences of each SST anomaly type is denoted by N. Note that the NEP box encompasses both the Atlantic Niño and Benguela Niño regions. There were 7 positive (1963, 1968, 1974, 1988, 1996, 1999, and 2008) and 11 negative (1967, 1976, 1977, 1978, 1980, 1982, 1983, 1992, 1997, 2004, and 2005) SAOD years from 1960 to 2009. In all SAOD years except 1999 and 1982, SAOD is preceded by $p' < 0$ ($p' > 0$) at the SWP, which represents 86% (91%) of the cases for the positive (negative) phase of the SAOD.

SST anomaly type	Positive phase	Negative phase	ΣN
Dipole	$[\sigma(\text{NEP}) \geq 0.5, \sigma(\text{SWP}) \leq -0.5]$, $N = 21$ (7)	$[\sigma(\text{SWP}) \geq 0.5, \sigma(\text{NEP}) \leq -0.5]$, $N = 22$ (11)	43 (18)
Equatorial	$[\sigma(\text{ATL3}) \geq 1.0, \sigma(\text{SWP}) \geq 0.0]$, $N = 0$ (1)	$[\sigma(\text{ATL3}) \leq -1.0, \sigma(\text{SWP}) \leq 0.0]$, $N = 0$ (1)	0 (2)
Tropical	$[\sigma(\text{NEP}) \geq 1.0, \sigma(\text{SWP}) \geq 0.0]$, $N = 0$ (0)	$[\sigma(\text{NEP}) \leq -1.0, \sigma(\text{SWP}) \leq 0.0]$, $N = 0$ (0)	0 (0)
Extratropical	$[\sigma(\text{SWP}) \geq 1.0, \sigma(\text{NEP}) \geq 0.0]$, $N = 0$ (1)	$[\sigma(\text{SWP}) \leq -1.0, \sigma(\text{NEP}) \leq 0.0]$, $N = 0$ (0)	0 (1)

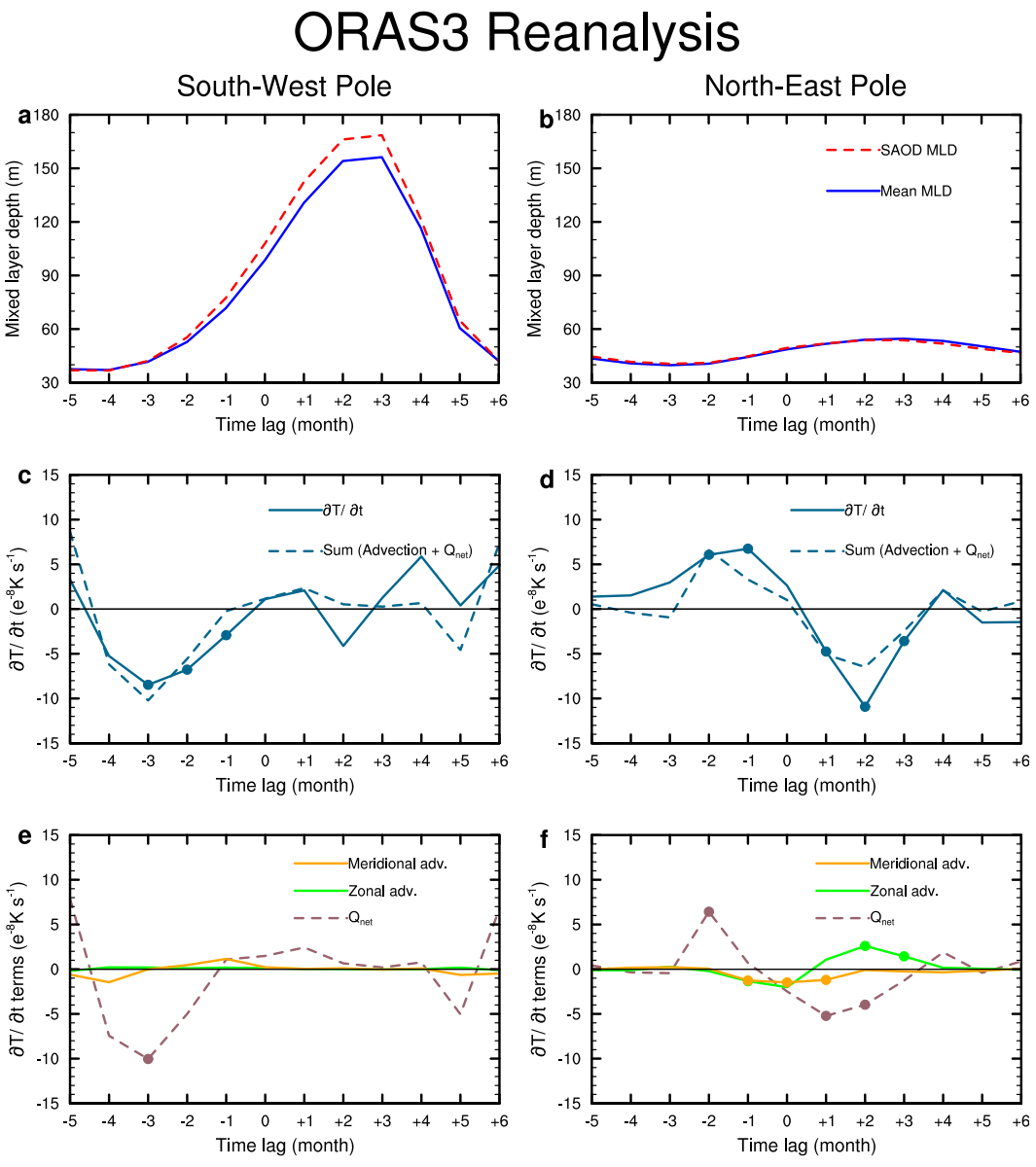

FIG. 5. Composite evolution of the ocean mixed layer heat budget associated with the SAOD over (left) the NEP and (right) the SWP in the ORAS3, 1960–2009. (a),(b) Climatological-mean annual cycle of MLD (solid blue curve) and MLD during the SAOD year (dashed red curve). (c),(d) Anomalies of temperature tendency ($\partial T/\partial t$; solid curve) and contributions from the advection and net heat flux terms (dashed curve). (e),(f) Anomalies of tendencies due to meridional temperature advection (yellow curve), zonal advection (green curve), and net heat flux (dashed purple curve). Dots indicate statistical significance at 95% confidence level. The composites are based on 10 positive SAOD events from HadISST determined by $+1.0\sigma$ of the index in June corresponding to lag = 0 from 1969 to 2009; these are 1963, 1966, 1968, 1971, 1974, 1988, 1996, 1998, 1999, and 2008. Note that as defined in Eq. (3), negative (positive) anomalies of the advection terms denote warming (cooling) of the ocean mixed layer; positive (negative) anomalies of the heat flux term represent warming (cooling) of the mixed layer.

temperature advection terms. Res is a residual term that represents the sum of unresolved physical processes (e.g., diffusion, entrainment at the base of the mixed layer, turbulent mixing, and high-frequency variability not resolved by the monthly time series analyzed here). In our calculations here, the vertical temperature advection term $w\partial T/\partial z$ is also included in Res because of the uncertainty often associated with its computation, and the contribution of equatorial upwelling is likely reduced by the meridional extent of the NEP (0°–15°S). Note that as

defined here, negative (positive) anomalies of the advection terms denote warming (cooling) of the ocean mixed layer; the reverse is the case for the heat flux term.

The depth of the MLD h is defined as the depth at which ocean temperatures are 0.5 K lower than those at the surface; thus, h changes in space and time. For each variable, $[\cdot]$ is computed as the vertical average over the ocean mixed layer:

$$[\cdot] = \frac{1}{h}\int_0^h dz. \tag{4}$$

Using the ORAS3 dataset, we computed the composite anomalies of the terms of Eq. (3) centered on June (when the boreal summer peak SST variability at both poles tends to occur; see Fig. 3) as the reference month (lag = 0). While some earlier studies suggest that the SASD peaks in boreal winter (e.g., Venegas et al. 1997; Morioka et al. 2011), the present analysis is focused on the SAOD, which peaks in summer, similar to the Atlantic Niño. Figure 3 [see also Fig. 2 of Nnamchi et al. (2011)] clearly shows that the SWP dominates in boreal winter, whereas the signal of the NEP or Atlantic Niño is comparatively small. As discussed in section 3a, it is only in boreal summer that the amplitudes of the SST variability are of similar magnitudes in the southwestern and eastern equatorial Atlantic Ocean.

The composite evolution of the anomalies of $\partial T/\partial t$ is closely reproduced by the sum of the surface net heat flux and advection terms at both the NEP and SWP during a typical SAOD year (Figs. 5c,d). Thus, the residual term (Res, which includes the $w\partial T/\partial z$ term) is quite small, especially at the SWP and prior to the peak phase of the SAOD. At the SWP, the cooling tendency reaches a maximum in March corresponding to lag −3 similar to the heat budget terms; a month later the budget terms peak at the NEP. There is a 1-month time lag between the sum of advection and heat flux terms and $\partial T/\partial t$ at the NEP, which could be due to the unresolved physical processes.

The initial cooling at the SWP is mainly attributable to heat flux anomalies that (similar to $\partial T/\partial t$) peak at lag −3 (Figs. 5e,f). Once this peak is reached, the cooling begins to reverse during the subsequent months. The peak anomalies at the SWP coincide with and enhance the seasonal deepening of the mixed layer. This both limits the growth of the SST anomalies and increases their persistence. Prior to the peak phase of the SAOD, the warming tendency at the NEP is also driven largely by heat flux peaking at lag −2. The advection terms are generally of smaller magnitudes and become robust (at lag −1) a month following the peak of Q_{net} and coincide with the peak phase of the SAOD event at lag = 0.

To check the robustness of these results, we repeated the heat budget calculations using the GECCO2 reanalysis for the same period: 1959–2009. As shown in Fig. 6, the Q_{net} peaks a month earlier (at $t - 4$) at the SWP and is comparatively less robust at the NEP. Note that while the ORAS3 has finer equatorial horizontal grids, this could be compensated for by the higher vertical resolution of the GECCO2, which appears to better resolve the seasonal cycle of the MLD. The result is that, overall, the key features of the SAOD heat budget are basically consistent in the two reanalysis datasets.

The time evolution of the anomalies at the NEP clearly follows the pattern of those calculated based on the Atlantic Niño region described in the modeling analysis of N15, which suggests that the SST anomalies could originate to a large extent from thermodynamic feedbacks and then coupled dynamics sets in to enhance the characteristic Niño-like spatial structure. Also, consistent with N15, Q_{net} anomalies play an important role for the evolution of the SST anomalies at the NEP. We note that there are some residual contributions (which may include the $w\partial T/\partial z$ term, entrainment, and other unresolved physical processes not accounted for in our analysis), that may in reality play significant roles in driving the SST anomalies, especially in the NEP region. For instance, vertical advection (including entrainment at the base of the ocean mixed layer) constitutes a key element for the seasonal development of the climatological-mean cold tongue. As discussed by Burls et al. (2011), an anomalous warming during the boreal summer will undoubtedly modify the "climatological Bjerknes feedback" associated with the cold tongue development. These unresolved physical processes account for nearly half of the anomalous warming at lag −1 at the NEP in both the ORAS3 and GECCO2 reanalyses. Nevertheless, a close examination of Figs. 5 and 6 shows that initial peaks in the $\partial T/\partial t$ term are clearly driven by the heat flux contribution and that accounting for the residuals at both poles should not change this.

There are no significant anomalies at either pole at lag −5 corresponding to January (Fig. 7). In the following months, the positive SST anomalies evolve incrementally at the NEP to reach statistical significance at lag −3 and a peak of approximately 0.50 K at lag = 0. On the other hand, weak positive SST anomalies persist at the SWP until lag −4, after which there is a phase change to negative values representing cooling that becomes significant at lag −2. The phase shift is characterized by a rapid plunge of the SST anomalies at the SWP under shallow mixed-layer conditions (for instance, there is ~0.44 K change in just 2 months between lags −4 and −2). This is then followed by a more gradual cooling (because of a rapid deepening of the ocean mixed layer

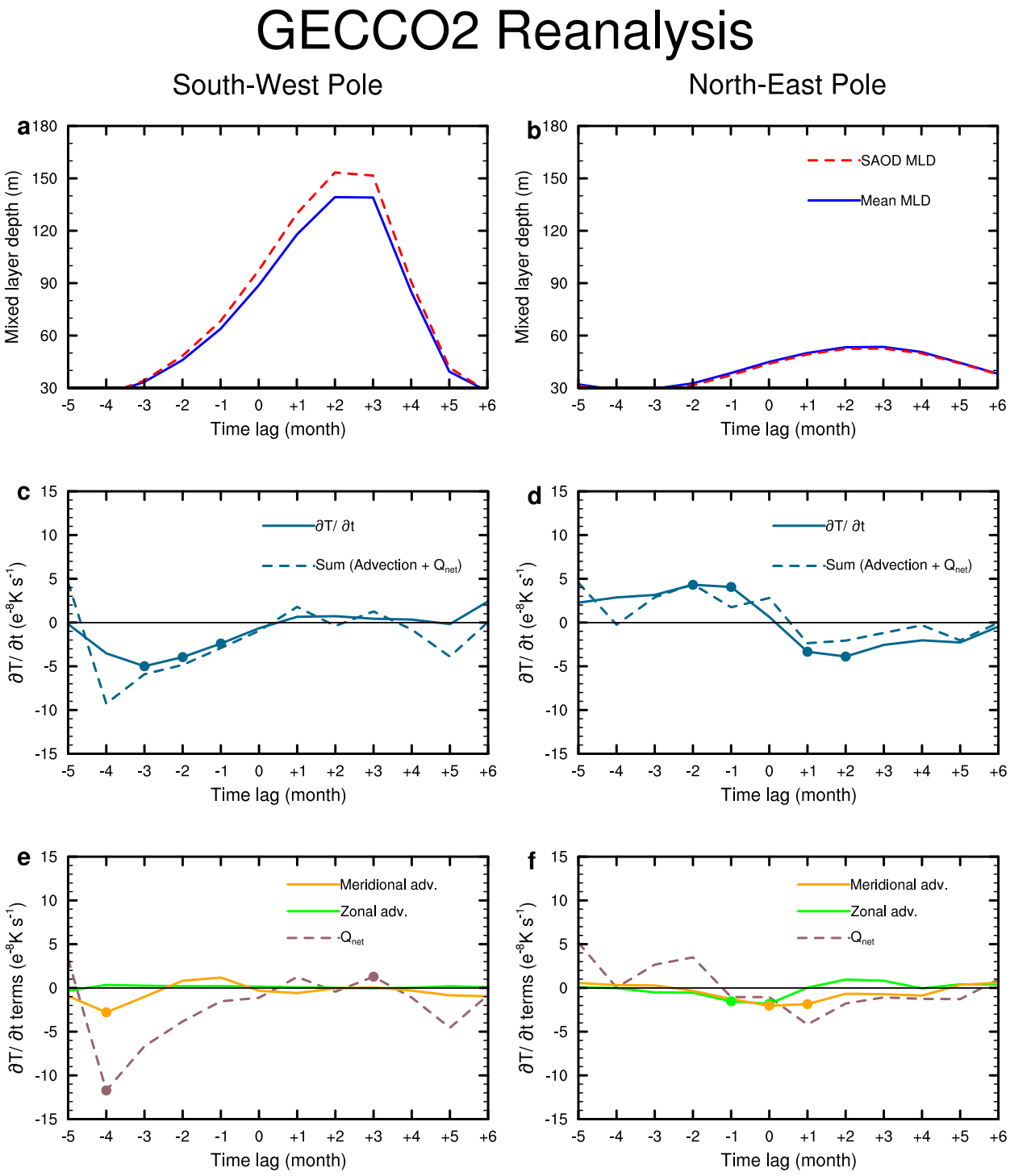

FIG. 6. As in Fig. 5, but based on the GECCO2 reanalysis, 1960–2009.

at a rate of ~20 m month^{-1}) until the peak of around −0.50 K is reached at lag = 0. In contrast, the mixed-layer is generally shallow (<60 m) and exhibits a comparatively weak annual cycle at the NEP, where dynamical coupling is also stronger. These differences in basic state and air–sea coupling mechanisms explain the rapid decrease of the $\partial T/\partial t$ and the heat flux terms at the SWP 2 months ahead of the peak anomalies at the NEP. From the budget analysis, we see the strongest negative $\partial T/\partial t$ at the SWP at lag −3 or −4 and then the anomalous

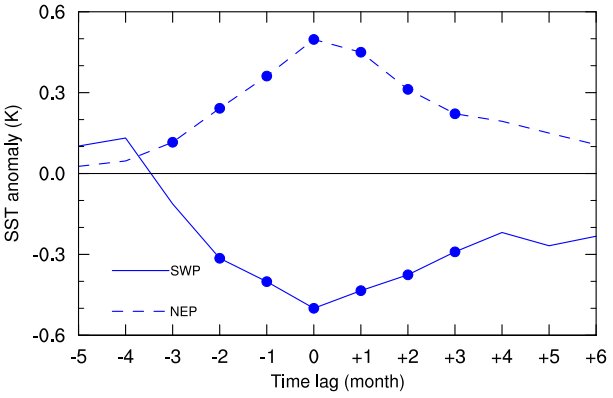

FIG. 7. Composite evolution of the domain-averaged SAOD-type HadISST anomalies, 1960–2009. Dashed (solid) curve shows the averages over the NEP (SWP) region. The composites are based on the SAOD index of $+1.0\sigma$; dots denote statistically significant ($P \leq 0.05$) anomalies.

tendencies weaken. This is consistent with a deepening mixed layer and also a reduction in the surface heat flux. The different evolution of the SST anomalies at the two poles is obviously consistent with the variability of $\partial T/\partial t$. In general, the SAOD heat budget shown here exhibits an evolution pattern similar to that of the Indian Ocean dipole in which the anomalies of $\partial T/\partial t$ and the sum of advection and heat flux at the eastern pole largely driven by heat flux lead those at the western pole with stronger dynamical coupling (Li et al. 2002).

b. *Thermodynamic feedbacks associated with the SAOD*

The above heat budget analysis suggests that the SAOD is largely driven by heat flux anomalies, rather than mixed layer temperature advection. To better understand the physical mechanism, we analyze the evolution maps of SST, Q_{net}, and wind stress anomalies leading to the peak phase of the SAOD in June. For these maps, we analyzed the composites for the same years used for the mixed layer heat budget calculations.

Figure 8 shows a progressive intensification of large-scale cyclonic anomalies over the South Atlantic Ocean from lag −4 to lag −2. The evolution appears better represented in the GECCO2 reanalysis, in which the robust easterly perturbations at 30°–40°S at lag −4 are complemented by equatorial westerly perturbations at lag −2. Considered in context of the mean state and as described in previous studies, the cyclonic anomalies represent a weakening of St. Helena subtropical anticyclone (Lübbecke et al. 2010; Richter et al. 2010; Lübbecke et al. 2014). Unlike these previous studies, however, here we emphasize the roles of Q_{net} anomalies in the evolution of the SST anomalies similar to N15, but using different spatial domains.

In the NEP region, the SST anomalies are restricted to the Benguela Niño area and are not directly connected to the Q_{net} anomalies at lag −4 in both ORAS3 and GECCO2 reanalyses. Lübbecke et al. (2010) shows that the Benguela Niño SST anomalies may be driven by remotely forced equatorial and coastal Kelvin waves, suggesting possible contributions from ocean dynamics at more regional scales. In the subsequent months, the Q_{net} anomalies strengthen at Benguela Niño and extend to the equatorial region, thereby intensifying the anomalous warming. Driven by the wind stress and Q_{net} anomalies, the progressive intensification of the SWP cooling anomalies and Niño-like warming in the near-equatorial region creates a distinct dipole structure at lag −2. From lag −4 to the peak phase of the SAOD at lag = 0, the axes of maximum and minimum SST anomalies undergo about 10°–15° northward shift linked to changes in wind stress and Q_{net} anomalies.

As shown in Figs. 5 and 6, the effects of ocean dynamics become significant toward the mature phase of the SAOD event at lag −1. The horizontal distribution of the associated anomalies reveals that at this time lag, the Q_{net} dampens the SST anomalies, extending from the southern extratropics to the equatorial belt (Fig. 8). Thus, there is a switchover of roles such that as from lag = 0, the equatorial dynamical coupling peaks and drives the SST anomalies while the heat flux anomalies cause a dampening effect. The phase shift at the NEP close to lag = 0 may tend to disguise the critical roles of the Q_{net} anomalies for the evolution of the SST anomalies during the preceding months while exaggerating the importance of ocean dynamics. This is not to say that ocean dynamics may not be important for the overall evolution of the coupled system, but one would expect ocean dynamics to be more important at regional scales such as in upwelling zones or regions of sharp SST gradients.

c. *A wind–evaporation–SST feedback hypothesis*

On the annual mean basis, the low-level atmospheric circulation over the South Atlantic is dominated by the St. Helena anticyclone centered at around 30°S. To the west, the SWP domain off the Brazil–Uruguay–Argentina coast is characterized by northwesterlies while southeast trade winds blow off the coast of Africa, in the NEP sector. Superimposed on the mean conditions are marked annual cycles in SST and zonal and meridional wind components at both centers of action of the SAOD (Fig. 9).

We determine an index of the potential capacity of atmospheric variability to excite the ocean mixed layer temperature anomalies at both poles during the course of the year as the monthly interannual standard deviations of the sea level pressure divided by the underlying MLD that it perturbs. We do this because we assume that the wind

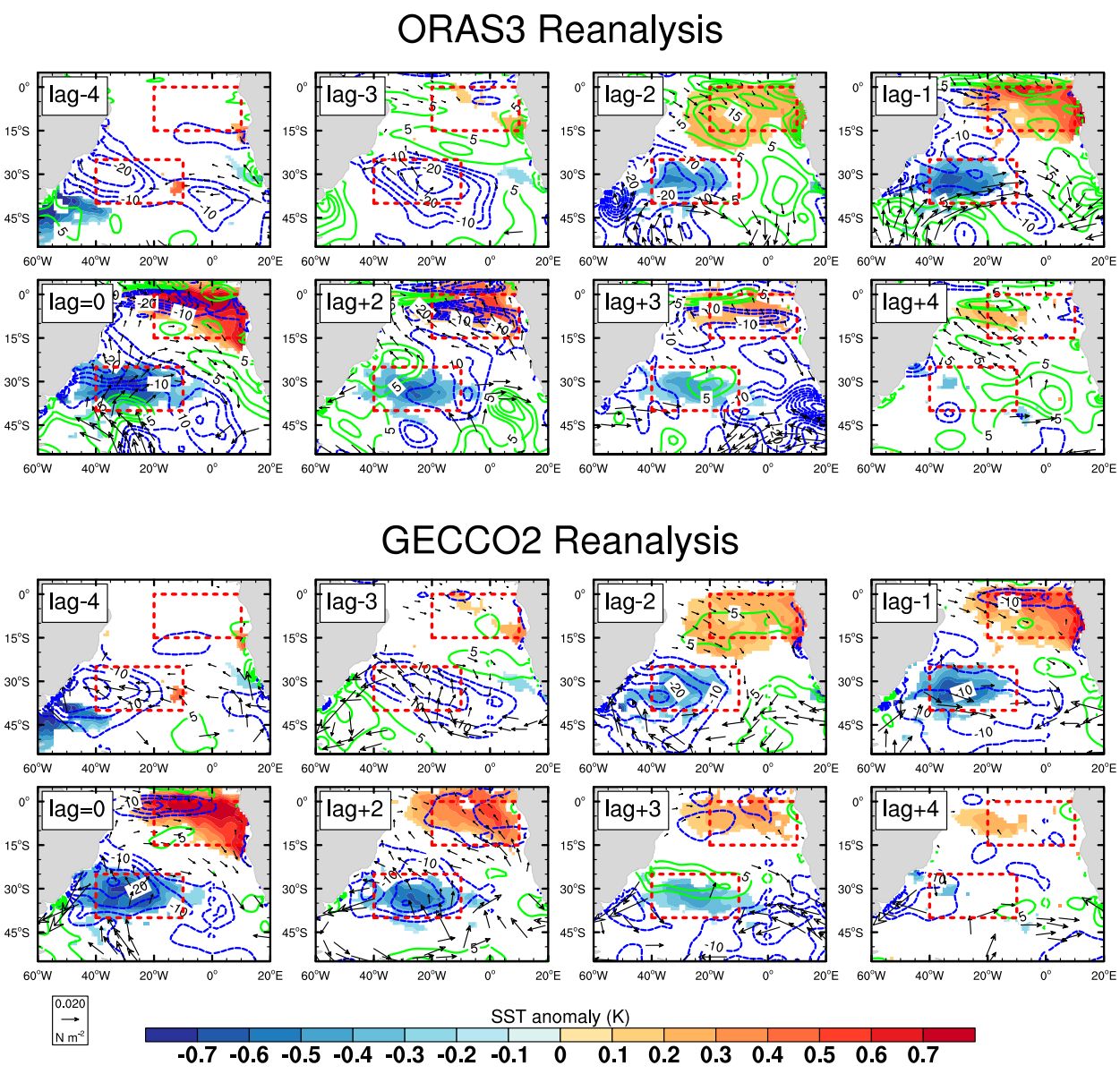

FIG. 8. Composite evolution maps of the anomalies of HadISST monthly SST (K; color scale), Q_{net} (W m^{-2}; contours), and winds stress (N m^{-2}; arrows) based on the SAOD index fixed at lag = 0, corresponding to June. Only statistically significant ($P \leq 0.05$) SST anomalies are shown, while significant ($P \leq 0.05$) wind stress anomalies are represented by thick black arrows. The Q_{net} is contoured at an interval of 5 W m^{-2}; positive anomalies shown by green contours indicate that the ocean mixed layer is gaining heat, and the negative anomalies (dashed blue contours) show that the ocean mixed layer is losing heat. The top (bottom) two rows of panels are based on the ORAS3 (GECCO2) dataset. All composites are based on the period 1960–2009.

variability and turbulent fluxes are proportional to the sea level pressure and that the mixed layer temperature is primarily driven by turbulent fluxes. This index generally exhibits more variability at the SWP, especially between December and March with a peak in February, suggesting that the South Atlantic extratropics has the greatest potential to excite SST anomalies during these months. Against this background, we outline a wind–evaporation–SST hypothesis through which the SAOD may originate.

Previous studies show that the weakening of the St. Helena anticyclone in boreal winter and spring months leads the Atlantic Niño the following JJA. Lübbecke et al. (2014) show that while anticyclonic anomalies in February–March are strongly linked to the negative phase of the Atlantic Niño events in JJA for the positive phase, the associated cyclonic anomalies in April–May are important. The authors explained these differences by the early onset of cold tongue development

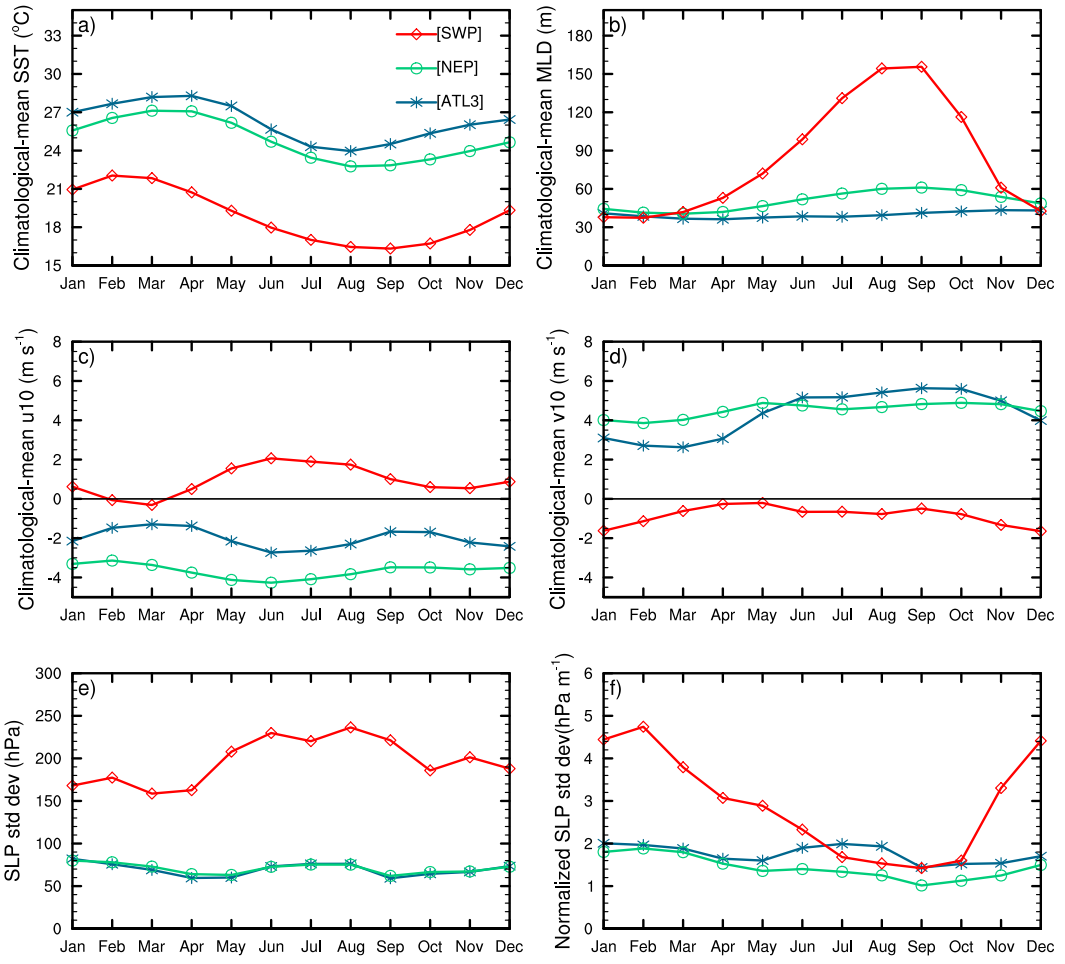

FIG. 9. Seasonal cycle over the equatorial subtropical South Atlantic Ocean, 1960–2009. (a) Observed climatological-mean SST, (b) climatological-mean ORAS3 ocean MLD, (c) climatological mean of reanalysis 10-m zonal winds, (d) climatological mean of reanalysis 10-m meridional winds, (e) standard deviation of reanalysis sea level pressure, and (f) standard deviation of reanalysis sea level pressure normalized by the climatological-mean MLD. Curves are based on domain averages over the NEP (green), ATL3 (blue), and SWP (red).

associated with the negative events, whereas the positive events are linked to delayed and suppressed seasonal cold tongue development.

Here, we have shown that in addition to the equatorial anomalies, the associated large-scale atmospheric fluctuations can equally exert robust effects on the southwestern Atlantic Ocean causing opposite SST anomalies. Consistent with Lübbecke et al. (2014), composite analysis reveals that weaker-than-normal sea level pressure ($p' < 0$) over the SWP during April–June preceded almost 86% of the observed equatorial Atlantic warming and extratropical cooling cases in JJA from 1960 to 2009 (see Table 2). Also, almost 91% of the observed equatorial Atlantic cooling and extratropical warming cases were preceded by anomalous high pressure ($p' > 0$) at the SWP during January–March. We repeated the analysis using the NCEP–NCAR reanalysis (Kalnay et al. 1996), and the results do not change, which adds to the robustness of these findings. We can infer from this event-based analysis that atmospheric anomalies at the SWP may explain most observed SAOD cases.

As the anticyclone weakens, the mean northerlies over the SWP also weaken. Blowing over comparatively warmer tropical ocean, the mean winds will typically tend to suppress evaporation on reaching the SWP because of the advection of warm and moist air from the equatorial region. Thus, as the winds relax during the evolution of the SAOD, evaporation is increased, leading to surface cooling (Figs. 5–8). Over the NEP, the prevailing southeast trade winds will tend to weaken because of a weakening of the anticyclone. In the mean state, this wind originates from the subtropics and tends to enhance cooling on reaching the NEP due to subsidence, evaporation, and equatorward advection (Seager et al.

2003). Thus, a weakening of these trade winds associated with the evolution of the SAOD will suppress evaporation, thereby causing net surface warming at the NEP.

Our results here show that the SAOD may be induced by atmospheric perturbations. On the other hand, earlier studies have demonstrated that an amplification of the zonal SST gradients (with cooling anomalies in the cold tongue and warming in the SWP regions, respectively) intensifies the anticyclone and associated atmospheric circulations (Seager et al. 2003; Richter et al. 2008). This suggests a two-way feedback between the SST gradients and large-scale atmospheric anomalies. The result is that SST anomalies at the two poles of the SAOD appear to reinforce each other through the interactions of the atmospheric anomalies with the ocean mixed layer.

More detailed analysis of the wind–evaporation–SST feedback outlined here is needed to confirm the importance of the mechanism for the evolution of the SAOD-type SST anomalies. There is also a possible role for cloud feedbacks. For instance, the modeling analysis of Bellomo et al. (2015) shows that enhanced cloud feedbacks over the Benguela Niño region increases SST anomalies in the Atlantic Niño region. Thus, further studies are also necessary to better understand the roles of cloud feedbacks on radiation and evolution of the SAOD anomalies.

5. Concluding remarks

The equatorial Atlantic cold tongue is subject to southern extratropical influence through perturbations of the St. Helena anticyclone and consequently the southeasterly trade winds (Robertson and Mechoso 2000). Our analysis shows that atmospheric anomalies excited by the perturbations of the anticyclone may trigger the evolution of an opposite phase in SST variability structure between the eastern equatorial and southwestern extratropical Atlantic Ocean (i.e., the SAOD). Event-based analysis shows that fluctuations of the anticyclone account for 16 of the 18 observed SAOD cases from 1960 to 2009.

Previous studies have shown that the evolution of SST anomalies from the southeastern Atlantic Ocean (the Benguela Niño sector) linked to fluctuations of the St. Helena subtropical anticyclone earlier in the year is associated with the equatorial Atlantic Niño during the boreal summer (Huang and Shukla 2005; Hu and Huang (2007); Lübbecke et al. 2010; Richter et al. 2010). Indeed, the Atlantic Niño is not purely an equatorial phenomenon as the SST anomalies are typically oriented toward the southeastern Atlantic Ocean. Our analysis here goes further to show that this near-equatorial pattern is consistently tied to an opposite phase over the southwestern Atlantic to the point that the two may be regarded as parts of the same climate mode—the SAOD, of which the Atlantic Niño is essentially the equatorial manifestation.

Ocean mixed layer heat budget shows that the SAOD is largely driven by the surface net heat flux partly controlled by (stochastic) atmospheric perturbations and possibly the systematic evolution of the wind–evaporation–SST feedback. Ocean dynamics seems to play a secondary role and is more important over the near-equatorial pole, particularly toward the mature phase of an event when heat flux dampens rather than drives the SST anomalies, a situation that may exaggerate (disguise) the roles of ocean dynamics (heat flux) in the overall evolution of the anomalies. Although there are several important processes such as vertical advection, entrainment at the base of the mixed layer, Ekman transport, and turbulent mixing (see Sterl and Hazeleger 2003; Haarsma et al. 2005) not accounted for in our analysis, the inclusion of these terms should not change the leading role of heat flux in driving the SAOD-type SST anomalies in the early part of its development. Furthermore, questions remain on the reliability of the reanalyses analyzed here because of possible biases in the models used to construct them and poor observational coverage of the South Atlantic Ocean. Despite these caveats, our results support the modeling analysis of N15 (which shows that the equatorial Atlantic SST anomalies are largely driven by the surface net heat flux anomalies consistent with a first-order autoregressive process) by describing how the equatorial anomalies form a part of a large-scale phenomenon, that is, the SAOD, originating from stochastic atmospheric perturbations from the southern extratropics.

Consistent with the foregoing discussion, previous studies based on purely thermodynamic ocean–atmosphere interactions (as present in the so-called slab ocean–atmosphere coupled models) identified a dipole structure as the leading mode of SST variability over the South Atlantic Ocean (Haarsma et al. 2005; Trzaska et al. 2007). A comparison of Figs. 2–4 of Haarsma et al. (2005) clearly shows that the dipole structure does not change much when the same atmospheric model is coupled to 1) the full ocean dynamics, 2) a 50-m deep passive thermodynamic ocean model, or 3) a thermodynamic ocean model in which Ekman transport, wind-induced mixing, and varying mixed layer depths are represented. However, the authors argue that the spectrum of the leading dipole structure in the slab model is more ''red'' because of the absence of the temperature advection terms. Advection may enhance the SST variance in the equatorial region (Nnamchi et al. 2015), although the southerly displacement of the anomalies in Haarsma et al. (2005) also applies to the fully coupled configuration of the model.

As shown in a seasonally stratified analysis [see Fig. 2 of Nnamchi et al. (2011)], the northern pole reaches the equatorial belt only in boreal summer; as would be expected from the northernmost migration of the St. Helena anticyclone in this season. Thus, the mean annual cycle may be crucial for the observed seasonal fluctuations of the northern pole, and Burls et al. (2011, 2012) discussed this in terms of ocean dynamics. The slab models in which the mean annual cycle of the ocean heat transport is constrained by observations may therefore capture the boreal summer peak of the dipole structure (Trzaska et al. 2007).

There is robust coherence between SST anomalies over the eastern equatorial and southwestern extratropical Atlantic at the interannual and decadal time scales. The respective regions may be useful for the deployment of observational platforms for targeted measurements of ocean–atmosphere features. Our analysis shows that the Atlantic Niño and SAOD indices may be used interchangeably for most applications. While focused studies within each individual region may be key to understanding detailed physical processes controlling the anomalies, the SAOD index that better resolves some decadal variability appears more suited for the analysis of long-term ocean–atmosphere variability. Further work is needed to understand the mechanism responsible for setting the seemingly robust decadal peak of the SAOD. More studies are also needed to determine how the evolution of ocean–atmosphere anomalies over the South Atlantic extratropics described in this study may enhance seasonal climate predictions in the tropical Atlantic region. In addition, understanding the relationship of the SAOD with Atlantic Niño [and SASD, which has been shown to be related to the Pacific El Niño (Kayano et al. 2013; Rodrigues et al. 2015)] may provide a new insight into the connection between climate variability over the tropical Atlantic and Pacific Oceans.

Acknowledgments. H.C.N. and N.S.K. were supported by the EU FP7/2007-2013 PREFACE Project (Grant 603521), and the Research Council of Norway (Grant 233680/E10) provided support for their collaboration. We thank the anonymous reviewers for insightful comments that helped us to improve the manuscript.

REFERENCES

Balmaseda, M. A., A. Vidard, and D. L. T. Anderson, 2008: The ECMWF Ocean Analysis System: ORA-S3. *Mon. Wea. Rev.*, **136**, 3018–3034, doi:10.1175/2008MWR2433.1.

Bellomo, K., A. C. Clement, T. Mauritsen, G. Rädel, and B. Stevens, 2015: The influence of cloud feedbacks on equatorial Atlantic variability. *J. Climate*, **28**, 2725–2744, doi:10.1175/JCLI-D-14-00495.1.

Brandt, P., A. Funk, V. Hormann, M. Dengler, R. J. Greatbatch, and J. M. Toole, 2011: Interannual atmospheric variability forced by the deep equatorial Atlantic Ocean. *Nature*, **473**, 497–500, doi:10.1038/nature10013.

Burls, N. J., C. J. C. Reason, P. Penven, and S. G. Philander, 2011: Similarities between the tropical Atlantic seasonal cycle and ENSO: An energetics perspective. *J. Geophys. Res.*, **116**, C11010, doi:10.1029/2011JC007164.

——, ——, ——, and ——, 2012: Energetics of the tropical Atlantic zonal mode. *J. Climate*, **25**, 7442–7466, doi:10.1175/JCLI-D-11-00602.1.

Carton, J. A., X. Cao, B. S. Giese, and A. M. Da Silva, 1996: Decadal and interannual SST variability in the tropical Atlantic Ocean. *J. Phys. Oceanogr.*, **26**, 1165–1175, doi:10.1175/1520-0485(1996)026<1165:DAISVI>2.0.CO;2.

Chang, P., L. Ji, and H. Li, 1997: A decadal climate variation in the tropical Atlantic Ocean from thermodynamic air-sea interactions. *Nature*, **385**, 516–518, doi:10.1038/385516a0.

——, Y. Fang, R. Saravanan, L. Ji, and H. Seidel, 2006: The cause of the fragile relationship between the Pacific El Niño and the Atlantic El Niño. *Nature*, **443**, 324–328, doi:10.1038/nature05053.

Colberg, F., and C. J. C. Reason, 2007: Ocean model diagnosis of low-frequency climate variability in the South Atlantic region. *J. Climate*, **20**, 1016–1034, doi:10.1175/JCLI4055.1.

Compo, G. P., and Coauthors, 2011: The Twentieth Century Reanalysis Project. *Quart. J. Roy. Meteor. Soc.*, **137**, 1–28, doi:10.1002/qj.776.

Deppenmeier, A.-L., R. J. Haarsma, and W. Hazeleger, 2016: The Bjerknes feedback in the tropical Atlantic in CMIP5 models. *Climate Dyn.*, doi:10.1007/s00382-016-2992-z, in press.

Deser, C., A. S. Phillips, and M. A. Alexander, 2010: Twentieth century tropical sea surface temperature trends revisited. *Geophys. Res. Lett.*, **37**, L10701, doi:10.1029/2010GL043321.

Florenchie, P., J. R. E. Lutjeharms, C. J. C. Reason, S. Masson, and M. Rouault, 2003: The source of Benguela Niños in the South Atlantic Ocean. *Geophys. Res. Lett.*, **30**, 1505, doi:10.1029/2003GL017172.

——, C. J. C. Reason, J. R. E. Lutjeharms, M. Rouault, C. Roy, and S. Masson, 2004: Evolution of interannual warm and cold events in the southeast Atlantic Ocean. *J. Climate*, **17**, 2318–2334, doi:10.1175/1520-0442(2004)017<2318:EOIWAC>2.0.CO;2.

Giannini, A., R. Saravanan, and P. Chang, 2003: Oceanic forcing of Sahel rainfall on interannual to interdecadal time scales. *Science*, **302**, 1027–1030, doi:10.1126/science.1089357.

Haarsma, R. J., E. J. D. Campos, W. Hazeleger, C. Severijns, A. R. Piola, and F. Molteni, 2005: Dominant modes of variability in the South Atlantic: A study with a hierarchy of ocean–atmosphere models. *J. Climate*, **18**, 1719–1735, doi:10.1175/JCLI3370.1.

Hu, Z.-Z., and B. Huang, 2007: Physical processes associated with the tropical Atlantic SST gradient during the anomalous evolution in the southeastern Ocean. *J. Climate*, **20**, 3366–3378, doi:10.1175/JCLI4189.1.

Huang, B., and J. Shukla, 2005: Ocean–atmosphere interactions in the tropical and subtropical Atlantic Ocean. *J. Climate*, **18**, 1652–1672, doi:10.1175/JCLI3368.1.

——, and Z.-Z. Hu, 2007: Cloud-SST feedback in southeastern tropical Atlantic anomalous events. *J. Geophys. Res.*, **112**, C03015, doi:10.1029/2006JC003626.

Kalnay, E., and Coauthors, 1996: The NCEP/NCAR 40-Year Reanalysis Project. *Bull. Amer. Meteor. Soc.*, **77**, 437–471, doi:10.1175/1520-0477(1996)077<0437:TNYRP>2.0.CO;2.

Kaplan, A., M. Cane, Y. Kushnir, A. Clement, M. Blumenthal, and B. Rajagopalan, 1998: Analyses of global sea surface

temperature 1856–1991. *J. Geophys. Res.*, **103**, 18 567–18 589, doi:10.1029/97JC01736.

Kayano, M. T., R. V. Andreoli, and R. A. Ferreira de Souza, 2013: Relations between ENSO and the South Atlantic SST modes and their effects on the South American rainfall. *Int. J. Climatol.*, **33**, 2008–2023, doi:10.1002/joc.3569.

Keenlyside, N. S., and M. Latif, 2007: Understanding equatorial Atlantic interannual variability. *J. Climate*, **20**, 131–142, doi:10.1175/JCLI3992.1.

Köhl, A., 2015: Evaluation of the GECCO2 ocean synthesis: Transports of volume, heat and freshwater in the Atlantic. *Quart. J. Roy. Meteor. Soc.*, **141**, 166–181, doi:10.1002/qj.2347.

Li, T., Y. Zhang, E. Lu, and D. Wang, 2002: Relative role of dynamic and thermodynamic processes in the development of the Indian Ocean dipole: An OGCM diagnosis. *Geophys. Res. Lett.*, **29**, 2110, doi:10.1029/2002GL015789.

Lübbecke, J. F., and M. J. McPhaden, 2013: A comparative stability analysis of Atlantic and Pacific Niño modes. *J. Climate*, **26**, 5965–5980, doi:10.1175/JCLI-D-12-00758.1.

——, C. W. Böning, N. S. Keenlyside, and S.-P. Xie, 2010: On the connection between Benguela and equatorial Atlantic Niños and the role of the South Atlantic anticyclone. *J. Geophys. Res.*, **115**, C09015, doi:10.1029/2009JC005964.

——, N. J. Burls, C. J. C. Reason, and M. J. McPhaden, 2014: Variability in the South Atlantic anticyclone and the Atlantic Niño node. *J. Climate*, **27**, 8135–8150, doi:10.1175/JCLI-D-14-00202.1.

Martín-Rey, M., B. Rodríguez-Fonseca, I. Polo, and F. Kucharski, 2014: On the Atlantic–Pacific Niños connection: A multidecadal modulated mode. *Climate Dyn.*, **43**, 3163–3178, doi:10.1007/s00382-014-2305-3.

Morioka, Y., T. Tozuka, and T. Yamagata, 2011: On the growth and decay of the subtropical dipole mode in the South Atlantic. *J. Climate*, **24**, 5538–5554, doi:10.1175/2011JCLI4010.1.

——, S. Masson, P. Terray, C. Prodhomme, S. K. Behera, and Y. Masumoto, 2014: Role of tropical SST variability on the formation of subtropical dipoles. *J. Climate*, **27**, 4486–4507, doi:10.1175/JCLI-D-13-00506.1.

Nnamchi, H. C., and J. Li, 2011: Influence of the South Atlantic Ocean dipole on West African summer precipitation. *J. Climate*, **24**, 1184–1197, doi:10.1175/2010JCLI3668.1.

——, and ——, 2016: Floods and droughts at the Guinea Coast in connection with the South Atlantic Dipole. *Dynamics and Predictability of Global and Regional High-Impact Weather and Climate Events*, J. Li et al., Eds., Cambridge University Press, 271–279.

——, ——, and R. N. C. Anyadike, 2011: Does a dipole mode really exist in the South Atlantic Ocean? *J. Geophys. Res.*, **116**, D15104, doi:10.1029/2010JD015579.

——, ——, I.-S. Kang, and F. Kucharski, 2013: Simulated impacts of South Atlantic Ocean Dipole on summer precipitation at the Guinea Coast. *Climate Dyn.*, **41**, 677–694, doi:10.1007/s00382-012-1629-0.

——, ——, F. Kucharski, I.-S. Kang, N. S. Keenlyside, P. Chang, and R. Farneti, 2015: Thermodynamic controls of the Atlantic Niño. *Nat. Commun.*, **6**, 8895, doi:10.1038/ncomms9895.

Patricola, C. M., R. Saravanan, and P. Chang, 2014: The impact of the El Niño–Southern Oscillation and Atlantic meridional mode on seasonal Atlantic tropical cyclone activity. *J. Climate*, **27**, 5311–5328, doi:10.1175/JCLI-D-13-00687.1.

Rayner, N. A., D. E. Parker, E. B. Horton, C. K. Folland, L. V. Alexander, D. P. Rowell, E. C. Kent, and A. Kaplan, 2003: Global analyses of sea surface temperature, sea ice, and night marine air temperature since the late nineteenth century. *J. Geophys. Res.*, **108**, 4407, doi:10.1029/2002JD002670.

Richter, I., C. R. Mechoso, and A. W. Robertson, 2008: What determines the position and intensity of the South Atlantic anticyclone in austral winter?—An AGCM study. *J. Climate*, **21**, 214–229, doi:10.1175/2007JCLI1802.1.

——, S. K. Behera, Y. Masumoto, B. Taguchi, N. Komori, and T. Yamagata, 2010: On the triggering of Benguela Niños: Remote equatorial versus local influences. *Geophys. Res. Lett.*, **37**, L20604, doi:10.1029/2010GL044461.

——, ——, ——, ——, H. Sasaki, and T. Yamagata, 2013: Multiple causes of interannual sea surface temperature variability in the equatorial Atlantic Ocean. *Nat. Geosci.*, **6**, 43–47, doi:10.1038/ngeo1660.

Robertson, A. W., and C. R. Mechoso, 2000: Interannual and interdecadal variability of the South Atlantic Convergence Zone. *Mon. Wea. Rev.*, **128**, 2947–2957, doi:10.1175/1520-0493(2000)128<2947:IAIVOT>2.0.CO;2.

Rodrigues, R. R., E. J. D. Campos, and R. Haarsma, 2015: The impact of ENSO on the South Atlantic subtropical dipole mode. *J. Climate*, **28**, 2691–2705, doi:10.1175/JCLI-D-14-00483.1.

Seager, R., R. Murtugudde, N. Naik, A. Clement, N. Gordon, and J. Miller, 2003: Air–sea interaction and the seasonal cycle of the subtropical anticyclones. *J. Climate*, **16**, 1948–1966, doi:10.1175/1520-0442(2003)016<1948:AIATSC>2.0.CO;2.

Servain, J., I. Wainer, J. P. McCreary Jr., and A. Dessier, 1999: Relationships between the equatorial and meridional modes of climatic variability in the tropical Atlantic. *Geophys. Res. Lett.*, **26**, 485–488, doi:10.1029/1999GL900014.

Siongco, A. C., C. Hohenegger, and B. Stevens, 2015: The Atlantic ITCZ bias in CMIP5 models. *Climate Dyn.*, **45**, 1169–1180, doi:10.1007/s00382-014-2366-3.

Smith, T. M., R. W. Reynolds, T. C. Peterson, and J. Lawrimore, 2008: Improvements to NOAA's historical merged land–ocean surface temperature analysis (1880–2006). *J. Climate*, **21**, 2283–2296, doi:10.1175/2007JCLI2100.1.

Sterl, A., and W. Hazeleger, 2003: Coupled variability and air-sea interaction in the South Atlantic Ocean. *Climate Dyn.*, **21**, 559–571, doi:10.1007/s00382-003-0348-y.

Subramaniam, A., C. Mahaffey, W. Johns, and N. Mahowald, 2013: Equatorial upwelling enhances nitrogen fixation in the Atlantic Ocean. *Geophys. Res. Lett.*, **40**, 1766–1771, doi:10.1002/grl.50250.

Tokinaga, H., and S.-P. Xie, 2011: Weakening of the equatorial Atlantic cold tongue over the past six decades. *Nat. Geosci.*, **4**, 222–226, doi:10.1038/ngeo1078.

Trzaska, S., A. W. Robertson, J. D. Farrara, and C. R. Mechoso, 2007: South Atlantic variability arising from air–sea coupling: Local mechanisms and tropical–subtropical interactions. *J. Climate*, **20**, 3345–3365, doi:10.1175/JCLI4114.1.

Venegas, S. A., L. A. Mysak, and D. N. Straub, 1996: Evidence for interannual and interdecadal climate variability in the South Atlantic. *Geophys. Res. Lett.*, **23**, 2673–2676, doi:10.1029/96GL02373.

——, ——, and ——, 1997: Atmosphere–ocean coupled variability in the South Atlantic. *J. Climate*, **10**, 2904–2920, doi:10.1175/1520-0442(1997)010<2904:AOCVIT>2.0.CO;2.

Wagner, R. G., and A. M. Da Silva, 1994: Surface conditions associated with anomalous rainfall in the Guinea coastal region. *Int. J. Climatol.*, **14**, 179–199, doi:10.1002/joc.3370140205.

Xie, S.-P., and J. A. Carton, 2004: Tropical Atlantic variability: Patterns, mechanisms, and impacts. *Earth's Climate: The Ocean–Atmosphere Interaction*, *Geophys. Monogr.*, Vol. 147, Amer. Geophys. Union, 121–142.

Zebiak, S. E., 1993: Air–sea interaction in the equatorial Atlantic region. *J. Climate*, **6**, 1567–1586, doi:10.1175/1520-0442(1993)006<1567:AIITEA>2.0.CO;2.